Modeling Meteoroid Densities for Spacecraft Risk Assessment

Steven Ehlert

Qualis Corporation, Jacobs Space Exploration Group, NASA Meteoroid Environment Office, Marshall Space Flight Center EV44,
Huntsville, Alabama, 35812, USA, steven.r.ehlert@nasa.gov

ABSTRACT

This report describes the methodologies and algorithms that NASA's Meteoroid Environment Office (MEO) currently utilizes to measure meteoroid densities. We discuss the needs for an accurate model for the meteoroid density distribution in its Meteoroid Engineering Model (MEM), and its potential implications for spacecraft design. The recently developed process is heavily derived from that of previous work [1], although subtle differences exist. A thorough comparison of the best-fit densities derived for sixty meteoroids in [1] and with the process described here shows that discrepancies in final densities larger than a factor of two are measured for $\sim 20\%$ of our test events. Such a level of discrepancy suggests that any density calculated using similar methods cannot be assumed to represent a unique fit to the data. Additional observational data for meteoroids beyond those utilized in this work will be essential for producing more reliable and repeatable density measurements.

1 INTRODUCTION

The density of a meteoroid plays a significant role in assessing the risk posed to any spacecraft unfortunate enough to sustain a meteoroid impact. For a fixed mass and speed, denser materials are able to more effectively penetrate the spacecraft and damage internal components [2, 3]. The higher risk associated with denser meteoroids may require thicker and more massive shielding to protect a spacecraft. Therefore, providing a more realistic model of meteoroid densities is a top priority for NASA's Meteoroid Environment Office (MEO).

Meteoroid densities are notoriously difficult to measure. There currently exists no means by which large samples of meteoroids can be collected and analyzed *in situ*, which would be the ideal method for measuring bulk densities. Some insights into the densities of meteoroids can be discerned by analyzing samples of meteorites that have survived reentry to the ground. The densities measured for meteorites range from carbonaceous chondrites ($\sim 2\,\mathrm{g\,cm^{-3}}$) to that of solid iron ($\sim 8\,\mathrm{g\,cm^{-3}}$). While these constitute direct measurements of the bulk material density, uncertainties persist because meteorites have undergone significant heating and ablation during their atmospheric entry. The bulk density of a meteorite as observed on the ground may not be identical to its bulk density prior to atmospheric entry. Even more problematic is the fact that meteorite producing events are such a small and biased fraction of all meteoroids. They are not representative of the underlying population encountered by spacecraft.

Since there exists no instrument that can measure meteoroid densities *in situ*, most efforts to model meteoroid densities have focused on modeling the ablation of meteors in the atmosphere. Physically, we expect meteoroids to have bulk densities in the range $\sim 0.1 - 8.0\,\mathrm{g\,cm^{-3}}$. The lower limit corresponds to extremely porous, loosely bound aggregates of grains. The upper limit corresponds to the density of solid iron. The most thorough and complete effort to model meteoroid densities to date was done by [1], which calculated densities for 92 ablating meteor events observed with optical cameras operating at video frame rates. From these observations, the density of the meteoroid was inferred by modeling the joint deceleration and radiative emission of the meteor during its ablation.

The determinations of [1] were utilized by the Meteoroid Engineering Model 3 (MEM 3) for characterizing the densities of the meteoroid environment. The previous version of MEM, MEMR2, assumed that every meteoroid had a density of $1\,\mathrm{g\,cm^{-3}}$. In MEM 3, the density distribution is modeled using two populations [4, 5]. One population corresponds to meteoroids with low densities ($\sim 0.85\,\mathrm{g\,cm^{-3}}$), while the other corresponds to meteoroids with higher densities ($\sim 3.8\,\mathrm{g\,cm^{-3}}$). The association of a meteoroid with one of these populations is based on its orbital Tisserand parameter, T_J. This parameter helps classify orbits based on their susceptibility to perturbations by Jupiter (hence the J in the subscript). As a rule-of-thumb, meteoroid orbits with $T_J < 2$ are associated with long period

comets, orbits with $2 \leq T_J \leq 4$ are typically associated with Jupiter family comets (JFC's), and orbits with $T_J > 4$ are generally associated with asteroidal orbits.

In this report, we describe the MEO's ongoing efforts to expand upon the work of [1] designed to improve the reliability of the meteoroid density distribution assumed for future versions of MEM.

2 METEOROID DENSITIES AND SPACECRAFT DESIGN

Before discussing the process of how meteoroid densities are modeled and determined, we will first describe one illustrative example as to how the density of a meteoroid impactor may affect spacecraft design and risk assessment. Assuming the modified Cour-Palais ballistic limit equation (BLE) [2] and aluminum target material properties of the Long Duration Exposure Facility (LDEF) assumed in [5], the maximum thickness of an aluminum plate that can be penetrated by a meteoroid is given as

$$t = 3.20\,\mathrm{cm} \times \left(\frac{d}{1\,\mathrm{cm}}\right)^{19/18} \left(\frac{\rho}{2.7\,\mathrm{g\,cm^{-3}}}\right)^{1/2} \left(\frac{v}{5.05\,\mathrm{km\,s^{-1}}}\right)^{2/3} \tag{1}$$

where d is the diameter of the meteoroid, ρ is the meteoroid's density, and v is the speed of the meteoroid normal to the target. The scaling relationships are illustrated in Figures 1 and 2 for several representative meteoroid diameters and speeds, respectively. For a fixed mass and speed, meteoroids associated with MEM 3's high density population can penetrate an aluminum plate roughly two times thicker than a meteoroid associated with MEM 3's low density population.

It is beyond the scope of this work to fully discuss what particular choices spacecraft designers may need to make in order to minimize risk, but these scaling relationships should make it clear that an accurate estimate of the relative contributions of lower and higher density meteoroid populations is crucial to properly estimating the risk posed by the meteoroid environment. Overestimating the contribution of high density meteoroids will result in missions that may have excessive shielding and mass that limits other capabilities. Underestimating this contribution may instead leave a spacecraft vulnerable to damage.

3 MODEL SETUP AND CALCULATIONS

The 92 densities derived by [1] and utilized by MEM 3 were determined by modeling the deceleration and mass loss of meteoroids observed using sensitive optical video camera systems. In the interest of increasing the total sample of meteoroid densities utilized for the density distribution, the MEO has undertaken a concerted effort to establish a revived version of the analysis procedure described in [1]. The process described below follows what was described in [1] as closely as possible, although some differences are inevitable given incomplete documentation. As a first test of this revived procedure, we attempted to reconstruct the density distributions of [1].

3.1 Observational Data

The data that we use to constrain these densities were optical video observations taken on individual nights between 2006 and 2009, and are described in detail in [1]. A total of 23 nights of usable video data were acquired using various camera systems, from which 92 meteoroid events that survived all data quality cuts were thoroughly analyzed. The fields of view of these systems ranged from $\sim 10^\circ - 35^\circ$. Each night of observation utilized cameras at least two sites separated by more than $40\,\mathrm{km}$, so that meteors detected in cameras at both sites could have their trajectories through the atmosphere calculated via triangulation. The trajectory calculations enable the meteor's geodetic latitude, longitude, and height to be determined as a function of time. The measurements of these three values as a function of time also enable the calculation of the meteoroid's instantaneous speed for every frame.

In addition to the trajectory data, the apparent magnitude of the meteor was calculated for each frame. These apparent magnitudes, when combined with the trajectory information, allow for the calculation of the meteor's absolute magnitude as a function of height. These calculations were performed by comparing the apparent brightness of the meteor to that of stars of known brightness contemporaneously located within the field of view.

Our first test of the revived procedure utilizes the exact same data as those used in the modeling efforts of [1]. We can therefore perform a direct comparison for the densities calculated for each event.

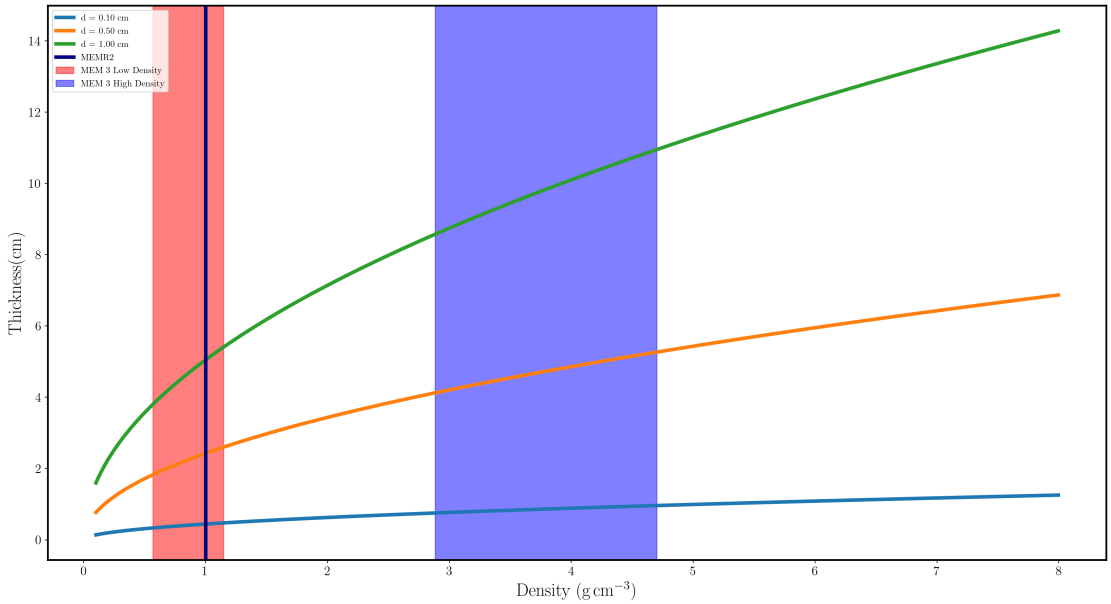

Fig. 1: Maximum thickness of aluminum (T6061 alloy, as deployed on LDEF) penetrated by a meteoroid impactor with a speed of $23\,\mathrm{km\,s^{-1}}$ as a function of density. Each curve denotes a different meteoroid diameter. The vertical line denotes the assumed density of all meteoroids MEMR2. MEM 3 assumes two populations of meteoroid densities, and are approximated by the shaded vertical regions.

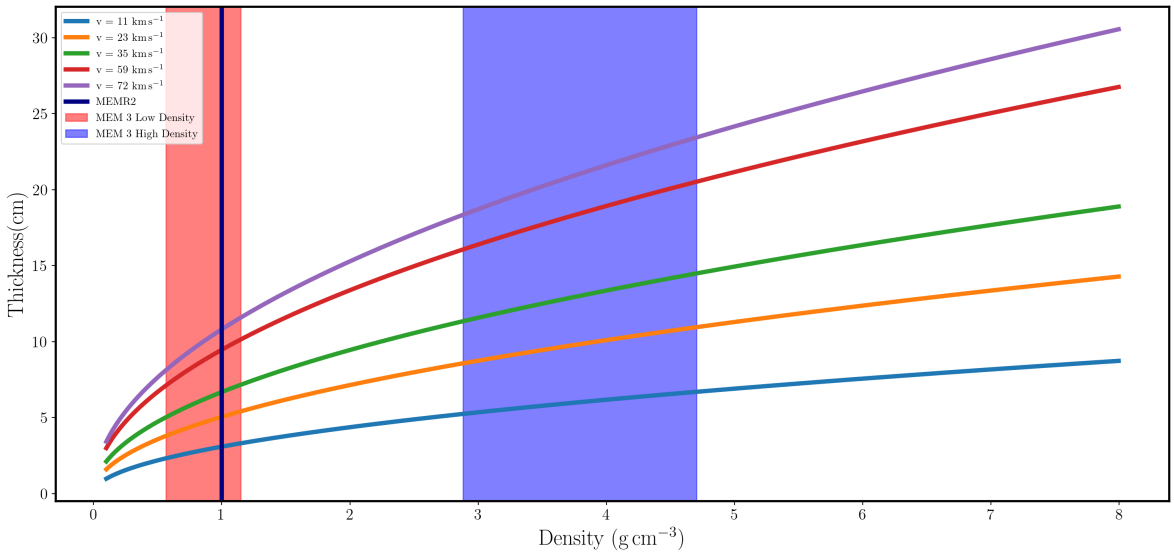

Fig. 2: Maximum thickness of aluminum (T6061 alloy, as deployed on LDEF) penetrated by a meteoroid impactor with a diameter of $1\,\mathrm{cm}$ as a function of density. Each curve denotes a different meteoroid speed. The vertical line denotes the assumed density of all meteoroids MEMR2. MEM 3 assumes two populations of meteoroid densities, and are approximated by the shaded vertical regions.

3.2 The Thermal Disruption Model

The observational data for all 92 meteoroids were then fit to the thermal disruption ablation model [6] in order to determine the meteoroid's bulk density. Fundamentally, the thermal disruption ablation model assumes that a meteoroid's composition is a "dust-ball' structure of many small, solid grains held together with a volatile "glue." The properties of the meteoroid during ablation are determined by solving a series of coupled, non-linear differential equations for its speed, height, temperature, mass loss, and radiative emission as a function of time. As the meteoroid ablates in the atmosphere, this dust-ball's "glue" can vaporize, causing instantaneous fragmentation and separation of a fraction of these grains. The separated grains then ablate apart from the main body. Rather than give a single initial mass for a meteoroid, the number of grains at a given mass is declared in the input. Any number of grains at distinct masses can be assumed, each with a user-determined number of grains. The initial total mass of the meteoroid is given as the sum of all grains. All of the details regarding the assumptions made by the model, the series of differential equations solved, and the available inputs can be found in [6].

3.3 Determination of a Best-Fit Density

The general goal of determining a density with this ablation model can be described as finding a variant of the thermal disruption model inputs that best fits the deceleration as a function of height, $v(H)$, and light curve data, $M(H)$, for an observed meteor event using the standard fit statistic χ^2 as a metric. How such a model is found in the continuum of possible models, however, presents a myriad of challenges. In order to make the parameter space more manageable, the input parameters were separated into two groups: one group of seven intensive parameters (which include the density, temperature of fragmentation, and specific heat of the meteoroid, among others) and the extensive parameters associated with the grain mass distribution.

Each of the spaces bound by these two groups is then explored using a "brute-force" grid search. For the first stage of the fitting process, an initial grain mass distribution and total mass are assumed, and then a low resolution grid search is performed over the seven-dimensional intensive parameter space. The best-fit model to the light curve and deceleration data is then identified using the reduced χ^2 statistic, and these intensive parameters are then fixed to these best-fit values in the second stage. In this second refinement stage, the grain mass distribution is adjusted to better fit the deceleration and light curve data. A total of 84,480 models were explored for each meteoroid event during the first stage of the broad search, and an additional $\sim 40,000$ models were explored during the second stage.

The choice of a "brute-force" grid search for these first two stages is necessary given the complexity of the thermal disruption model. Simple fitting algorithms that assume linear models and Gaussian-distributed uncertainties on the measurements, which invert the covariance matrix of the data, are entirely inappropriate for the non-linear behavior of the thermal disruption model. The challenge of non-linear least-squares optimization is even more severe for this model in particular, as the inclusion of fragmentation leads to large changes in model predictions as individual parameters are varied. Practically speaking, this leads to discontinuities in the fit statistic as parameters are varied (i.e., $\frac{d\chi^2}{d\alpha}$ is not continuous for a given model parameter α). Subsequently, minimization algorithms that attempt to exploit gradients in the fit statistic like steepest-descent or Levenberg-Marquardt [7] are unsuitable for exploring the parameter space. The grid search utilized here is robust to these concerns since it makes no assumptions about the variation of χ^2 across the parameter space.

3.3 Obtaining the Final Density

Despite serious efforts to automate the process of measuring meteoroid densities, the final solution for the best-fit density must have a manual inspection and adjustment stage. For some meteor events, none of the models in the two-stage grid search may provide objectively "good" fits to the data. The small number of values sampled for each intensive parameter in the grid searches may overlook models that may fit the data even better. No matter how "good" a fit the two-stage grid search may provide, the resultant model should always be manually inspected for quality and feasibility. A manual refinement stage is also performed in [1], although any repeatable details of that process are lacking documentation. For this work, a custom graphical user interface (GUI) was developed to help manually explore the entire parameter space. This GUI enables every parameter of the thermal disruption model to be tweaked at much finer precision than the grid search stages permit, as well as quickly identify how those small changes to the model parameters change the overall quality of the model fit.

4 CHALLENGES WITH MODELING AND FITTING DATA

As previous sections have discussed, the large number of parameters and presence of fragmentation in the thermal disruption model demand that an inefficient "brute-force" grid search[1] be run for each event in order to explore the parameter space. An even larger challenge with this modeling procedure also presented itself throughout this study, which severely limits the interpretation of the best-fit density measurements derived in this work.

While the thermal disruption model's many parameters are sufficiently flexible to describe the diversity in meteoroid light curves, that flexibility can lead to degeneracies where models with very different input parameters produce indistinguishable deceleration curves and light curves. The most severe parameter degeneracy identified for this model is between the grain mass distribution and the density. There exist an uncountable number of ways to distribute the total mass of the meteoroid between grains of discrete masses, even when the number of grain masses and the grain mass index are both fixed. Each variant of the grain mass distribution has a different deceleration curve and light curve, and each of these variants will require a different density to fit the observational data (i.e., the heights where ablation is observed to occur). For distributions with fewer numbers of more massive grains, lower densities better fit the data, whereas higher densities are necessary for larger numbers of smaller grains. Neither the specific grain masses assumed nor the grain mass index can be usefully constrained by this observational data set, as the individual grains are not spatially resolved by the cameras during ablation.

4.1 Comparison to Past Results

In order to demonstrate the extent to which these model degeneracies affect the final density measurements, we ran the process described above on a total of sixty events modelled in [1]. Special care was taken to perform the modeling efforts "blind" to the corresponding results of [1], in order to avoid unconsciously or deliberately biasing the manual refinement stages. It is crucial to note that the observational data and ablation model are essentially identical for this work and that of [1]. All that differs between the two analyses are the details regarding how the vast parameter space is explored.

The results of this cross-calibration exercise can be found in Figures 3 and 4. Figure 3 shows how the measurements for each individual event compare between [1] and this work, while Figure 4 shows the implications as to how the density distributions utilized in MEM 3 differ using the newly derived densities. The best-fit affine model comparing the densities measured in this work (E19) to those of [1] is

$$\rho_{E19} = (0.77 \pm 0.12)\rho_{K11} + (356 \pm 304) \tag{2}$$

suggesting that these densities are slightly lower than [1] on average. Individual events measured in this work were found to be significantly higher and lower than the measurements of [1]. Figure 3 shows that $\sim 20\%$ of the events show serious (greater than a factor of two) discrepancies between the past measurements of [1] and those measured here. From the standpoint of χ^2 values for each event, the differences are not large enough to favor the results of this report over [1] or vice versa - both models are formally "good" fits to the data based on their reduced value of χ^2. This degeneracy can be best visualized in Figures 5 and 6. Figure 5 shows the best fit models of [1] and this work for an event where the measured densities were in good agreement with one another given the published uncertainties in [1], while Figure 6 shows the best fit models for a second event with models where the density measured in this work is a factor of two lower than that published by [1]. This factor of two in density corresponds to the difference between a meteoroid with a density similar to a lump of coal and one that is solid aluminum.

Even more significant than the existence of these large outliers are the implications that these new best-fit densities have on the density distribution as modeled in MEM 3. The measured densities of [1], as shown in Figure 4, showed a clear separation between low density and high density meteoroids based on their Tisserand parameter. While meteoroids on orbits with $T_J < 2$ have similar density distributions in this work and in [1], the same cannot be said for meteoroids on orbits with $T_J > 2$. For these orbits, the events had modeled densities spanning the entire physically acceptable range of $\sim 0.1 - 8\,\mathrm{g\,cm^{-3}}$.

The fact remains that densities performed with a pipeline like this are practically impossible to consistently

[1] Although the precise run time of each stage of the grid search varies greatly with entry speed, mass, and zenith angle, each of the two stages takes approximately 8-24 hours of computation time to complete.

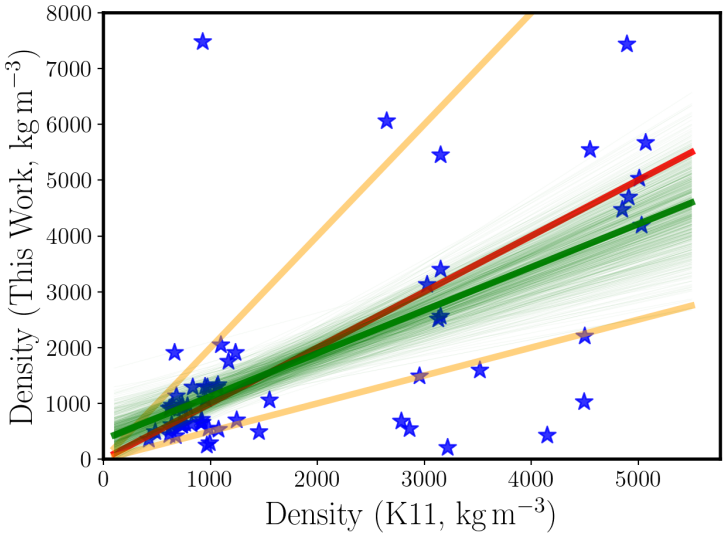

Fig. 3: Results of the cross-calibration of sixty events modelled by [1] using the newly developed density pipeline discussed in this report. The density of each event as measured by [1] can be found on the x-axis, and the corresponding density measured in this work is found on the y-axis. The red line denotes unity (i.e., $y = x$), while the orange lines denote a factor of two discrepancy (i.e., $y = 2x$ and $y = 0.5x$) curves. The darker green line denotes the best fit affine model, with fainter green lines denoting the uncertainties on the affine model.

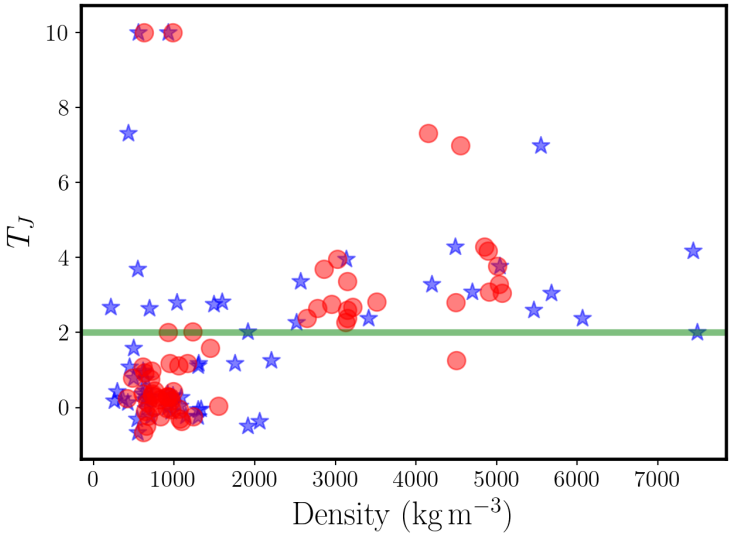

Fig. 4: Tisserand parameter as a function of meteoroid density of 60 events analyzed in [1]. The red circles denote the measurements of [1], while the blue stars are the measurements derived in this work. The green horizontal line denotes $T_J = 2$, the dividing line between the low density and higher density populations in MEM 3.

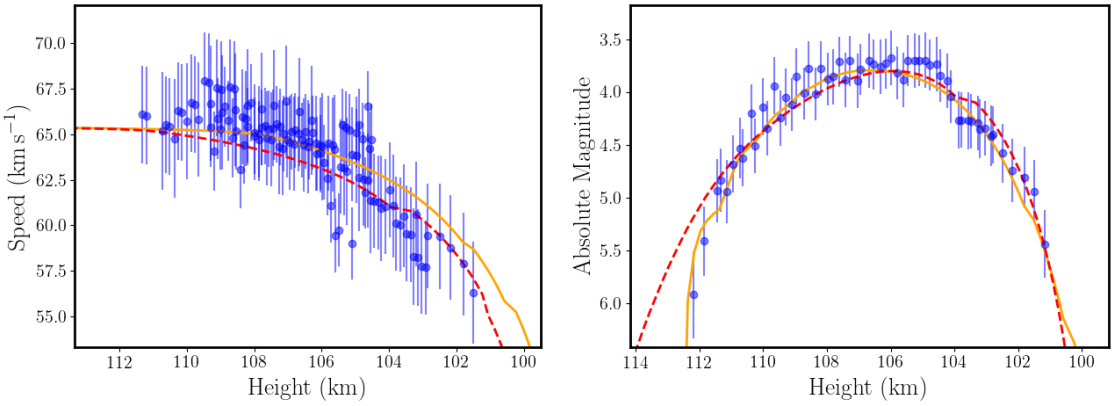

Fig. 5: Deceleration and light curve data for a meteor that was observed at 06:18:49 UTC on the morning of 2007-04-22. The orange curves denote the model derived in this work, which has a density of $0.984\,\mathrm{g\,cm^{-3}}$. The red dashed curves denote the model of [1], which has a density of $0.730^{+0.600}_{-0.200}\,\mathrm{g\,cm^{-3}}$. The two model determined densities are consistent with one another given the uncertainties quoted in [1].

reproduce. There exist numerous combinations of model input parameters with dramatically different densities that all provide similarly good fits to the data. The initial assumptions as to the grain masses, their distributions, and the other parameters will greatly influence which of these models is ultimately chosen after exploring the parameter space, and there are few constraints from the data as to which grain masses should be chosen. Even if the grid searches began with the exact same settings as those utilized in [1], both past work and this work required manual refinement and exploration through the parameter space. The particular choices of the manual search stages fundamentally cannot be repeated. No unique density can be determined without more stringent prior constraints or assumptions regarding the grain mass distribution of these events.

5 FUTURE PROSPECTS

The high level of degeneracy between model parameters is a basic reality of the thermal disruption ablation model. Different choices for the assumed grain mass distribution and density can result in nearly identical deceleration curves and light curves that fit the observational data equally well, despite the fact that their assumed densities may differ significantly. In the absence of any additional observational data or prior constraints, the resultant densities of [1] and this work should NOT be assumed to represent a unique solution. In fact, the cross calibration efforts between [1] and this work should suggest that a large range of models, each with a different density, could describe these data equally well.

Establishing more robust meteoroid density measurements requires additional observational data beyond the deceleration curve and light curve. Ideally, these measurements would provide direct constraints on the constituent grain masses and their distribution. In the context of measuring meteoroid densities, those dimensions appear to be the crucial degeneracy limiting the interpretation of any thermal disruption model fit. Comparing the other parameters of each best-fit model between the work of [1] and this work suggests that the other intensive parameters have less influence over the best-fit density than the grain mass distribution.

One promising path forward utilizes the extremely high resolution observations taken with the Canadian Automated Meteor Observatory (CAMO) at the University of Western Ontario [see 8–11, for a description of the camera system]. The $\sim 3\,\mathrm{m}$ spatial resolution of CAMO's camera will enable greatly improved density measurements. The improved spatial resolution of the CAMO observations will provide significantly higher precision measurements of deceleration, which in turn will better discriminate between different realizations of the thermal disruption model. Furthermore, the ability of CAMO to image the fragmentation process may offer the necessary breakthrough needed to break these model degeneracies. Such imagery of the fragmentation process could be used to directly image the

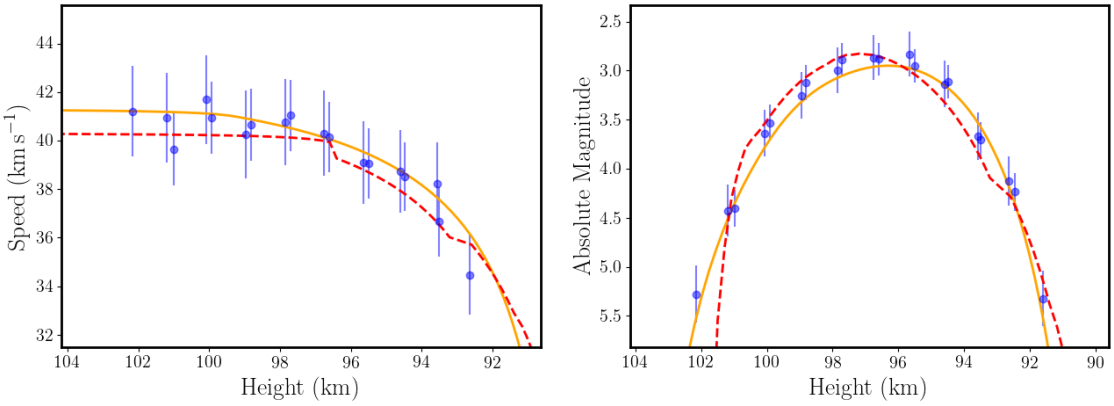

Fig. 6: Deceleration and light curve data for a meteor that was observed at 05:33:13 UTC on the morning of 2009-06-25. The orange curves denote the model derived in this work, which has a density of $1.495\,\mathrm{g\,cm^{-3}}$. The red dashed curves denote the model of [1], which has a density of $2.950^{+0.500}_{-0.200}\,\mathrm{g\,cm^{-3}}$. Despite the factor of ~ 2 discrepancy in their densities, both of these models provide similar fits to the deceleration curve and light curve data.

emission from fragments trailing in the wake of the main body's ablation. The additional measurements of the meteoroid's wake during ablation afforded by CAMO can be used to constrain the masses of the fragments and subsequently the initial grain mass distribution of the meteoroid independent of its deceleration and light curve. These measurements in turn will greatly reduce the size of the parameter space that needs to be explored and the number of viable densities that accurately reproduce the observations. These additional constraints and smaller parameter space will also reduce the necessity to which the modeling efforts will require manual refinement and inspection stages.

6 CONCLUSIONS

This manuscript describes new estimates of meteoroid densities utilizing the thermal disruption ablation model of [6] and the observational data of meteor events described in [1]. While the ablation model and data utilized in both [1] and this work were essentially identical, different choices were made in each work as to how to explore the vast parameter space. Unfortunately, assumptions regarding the initial grain mass distribution and how to explore the parameter space greatly impact the final results. Access to incomplete documentation as to what choices were made and how they were chosen in [1] limited the extent to which this work could faithfully reproduce the past procedure.

Approximately 20% of the events analyzed in this report show discrepancies with [1] that exceed a factor of two, with the new density pipeline providing measurements that are both significantly lower and higher than those measured in [1]. While factors of two are frequently an acceptable level of discrepancy in astronomy research, the engineering implications with regards to spacecraft risk and damage of this level of discrepancy cannot be ignored.

The newly calculated density distribution for meteoroids on orbits with $T_J > 2$ is significantly broader and more uniformly distributed than that found by [1]. The distributions of densities for meteoroids on orbits with $T_J \leq 2$ derived in [1] and in this work are similar to one another, with most values concentrated around $\sim 1\,\mathrm{g\,cm^{-3}}$.

More robust and reliable values of meteoroid densities will require a more extensive set of observations than those of [1]. In particular, stronger constraints on the grain mass distribution will be essential for a next generation density modeling effort. This work clearly demonstrates that differences in the assumed grain masses and their distribution can result in models with vastly different densities fitting the observational data equally well. The MEO is currently developing the methodologies needed to exploit new observations that may be able to break these degeneracies and greatly increase the repeatability of the modeling efforts.

7 ACKNOWLEDGEMENTS

We are thankful for the gracious support and encouragement of Dr. Margaret Campbell-Brown and Dr. Peter Brown, who both developed the thermal disruption model and assisted in the process of determining and reviewing some of the particular choices made by the current pipeline. These results made great use of the GNU parallel tool [12] in order to maximize computational throughput. Finally, we wish to thank Anne Diekmann (Jacobs Space Exploration Group) for her great assistance with Python GUI's. Without her help the GUI used to refine density measurements would not exist, and the manual refinement stages would have been prohibitively slow.

8 REFERENCES

1. Kikwaya, J. B., Campbell-Brown, M. & Brown, P. G. Bulk density of small meteoroids. A&A, Vol. 530, A113 (**June 2011**).
2. Hayashida, K. B. & Robinson, J. H. Single wall penetration equations. NASA/TM-103565, (**Dec. 1991**).
3. Watts, A. J. & Atkinson, D. *Dimensional scaling for impact cratering and perforation* in *LDEF: 69 Months in Space. Third Post-Retrieval Symposium* (**Feb. 1995**), 523–535.
4. Moorhead, A. V. *et al.* A two-population sporadic meteoroid bulk density distribution and its implications for environment models. Monthly Notices of the Royal Astronomical Society, Vol. 472, 3833–3841 (**Dec. 2017**).
5. Moorhead, A. V., Kingery, A. & Ehlert, S. NASA's Meteoroid Engineering Model (MEM) 3 and its ability to replicate spacecraft impact rates. arXiv e-prints, arXiv:1909.05947. arXiv: 1909.05947 [astro-ph.EP] (**Sept. 2019**).
6. Campbell-Brown, M. D. & Koschny, D. Model of the ablation of faint meteors. A&A, Vol. 418, 751–758 (**May 2004**).
7. Bevington, P. R. & Robinson, D. K. *Data reduction and error analysis for the physical sciences* (**2003**).
8. Subasinghe, D., Campbell-Brown, M. D. & Stokan, E. Physical characteristics of faint meteors by light curve and high-resolution observations, and the implications for parent bodies. Monthly Notices of the Royal Astronomical Society, Vol. 457, 1289–1298 (**Apr. 2016**).
9. Subasinghe, D., Campbell-Brown, M. & Stokan, E. Luminous efficiency estimates of meteors -I. Uncertainty analysis. Planetary and Space Science, Vol. 143, 71–77. arXiv: 1704.08656 [astro-ph.EP] (**Sept. 2017**).
10. Subasinghe, D. & Campbell-Brown, M. Luminous Efficiency Estimates of Meteors. II. Application to Canadian Automated Meteor Observatory Meteor Events. The Astronomical Journal, Vol. 155, 88. arXiv: 1801.06123 [astro-ph.EP] (**Feb. 2018**).
11. Subasinghe, D. & Campbell-Brown, M. Properties of meteors with double-peaked light curves. Monthly Notices of the Royal Astronomical Society, Vol. 485, 1121–1136. arXiv: 1902.05931 [astro-ph.EP] (**May 2019**).
12. Tange, O. *GNU Parallel 2018* ISBN: 9781387509881. https://doi.org/10.5281/zenodo.1146014 (Ole Tange, **Mar. 2018**).